MDPI

Antibacterial Activity and Bioactivity of Zn-Doped TiO$_2$ Coating for Implants

Binbin Kang [1] , Dongmei Lan [2], Lei Liu [1], Rui Dang [3], Chao Yao [2], Ping Liu [1], Fengcang Ma [1], Shengcai Qi [3,4,*] and Xiaohong Chen [1,*]

1   School of Materials and Chemistry, University of Shanghai for Science & Technology, Shanghai 200093, China
2   Medical College, Anhui University of Science and Technology, Huainan 232002, China
3   Department of Prosthodontics, Shanghai Stomatological Hospital, Fudan University, Shanghai 200437, China
4   Shanghai Key Laboratory of Craniomaxill of Acial Development and Diseases, Fudan University, Shanghai 200437, China
*   Correspondence: dentisitqi@163.com (S.Q.); xh_chen22@163.com (X.C.)

Abstract: Lacking osseointegration and peri-implantitis induced by bacterial infiltration are the pivotal issues for the long-term clinical success of implants. In order to improve the bioactivity and antibacterial properties of implant materials, volcano-shaped microporous TiO$_2$ coatings doped with Zinc (Zn) were fabricated via a micro-arc oxidation (MAO) method on pure titanium (Ti). The microstructure, morphology, and chemical composition of the Zn-doped coatings were systematically studied. In cell culture tests, the formed coatings promoted the adhesion and proliferation of bone mesenchymal stem cells (BMSCs), exhibiting good biocompatibility. The antibacterial experiments revealed that Zn-TiO$_2$ coatings possess excellent antibacterial properties against Staphylococcus aureus (*S. aureus*) and Porphyromonas gingivalis (*P. gingivalis*).

1. Introduction

Titanium (Ti) and its alloys are used in orthopedics, cardiovascular medicine, dentistry, and other applications because of their excellent mechanical properties and biocompatibility [1]. However, in recent years, several clinical issues, such as biomaterial-associated infections, peri-implantitis, and prosthetic joint infections, have been reported for Ti [2]. The biofilm formation due to bacterial adhesion was recognized as the major cause of these infections [3]. Once a biofilm is formed, pathogens are difficult to eliminate. The only way to solve the problem is to remove the contaminated implant from the patient. Prevention is the most effective approach to prevent implant-associated infections with antibacterial surface implants [4]. Therefore, antimicrobial surface coatings have attracted much attention due to the development of their surface properties to prolong the service life of implants.

There are many methods to modify the surface of a dental implant, such as HA coating, titanium plasma spray, sandblasted large-grit and acid-etching, micro-arc oxidation (MAO), etc. Among these methods, micro-arc oxidation (MAO) is one of the cost-effective and versatile ways to modify the surface of metallic implants with complex geometries [5]. MAO is a relatively simple technique with low cost compared to other surface modification methods. It can produce an oxide ceramic layer in situ on a metal substrate [6,7]. The TiO$_2$ coating fabricated by MAO is generally on the micro/nanoscale, which can significantly reduce the elasticity modulus of Ti [8]. These porous structures can also reduce the elastic modulus of the implant surface, promote bone cell adhesion, and enhance implant–bone bonding [9]. In addition, a porous-structure coating prepared by MAO has been proven to favor cell adhesion and proliferation [10,11]. MAO results in a changed surface topography

and a controllable thickness of the native oxide layer, which is suitable for osseointegration. The most striking characteristic of MAO is the formation of interconnecting pores, which can increase protein adsorption and stimulate osteoblast migration, resulting in faster osseointegration [12]. Some elements can be easily incorporated into the surface of titanium-based coatings via MAO, conferring dual functionalization and improving the compatibility of titanium alloys' characteristics, such as their antibacterial properties and biocompatibility [13].

Antibacterial agents, such as antibiotics [14], organic cation compounds [15], and metal elements [16,17], have been incorporated on the implant surface to prevent the formation of biofilm. Among them, Zinc (Zn) is known as one of the most effective agents because of its excellent antibacterial effects. In addition, Zn is an important trace element for the human body, which can enhance cell proliferation, osteoblast marker gene expression, osteogenic function, and alkaline phosphatase (ALP) activity [18,19]. Although Zn possesses excellent antibacterial properties, it also exhibits a high cytotoxic threshold [20]. Excessive zinc doping will cause cytotoxic effects in osteoblasts, while moderate zinc doping can promote the osteogenic differentiation of cells [21]. Hence, the quantitative control of the incorporation of Zn will achieve a dual function on the Ti surface by MAO.

P. gingivalis is recognized as being most closely related to the development of peri-implantitis and even the ultimate loss of dental implants [22]. *S. aureus* is a frequent commensal of the nares and skin and is considered a transient oral resident, which is identified at higher numbers in biofilm obtained from implants with peri-implantitis than in healthy peri-implant conditions [23,24]. The biological rationale of *S. aureus.* in peri-implantitis is the capacity to attach onto titanium surfaces [25] and contribute to biofilm-associated and medical-device-related infections [26]. Therefore, an evaluation of the antibacterial effects of implants against *P. gingivalis* and *S. aureus* can determine its scope of application.

In this study, Zn-incorporated coatings (Zn-MAO) on the dental implant surface were prepared by a micro-arc oxidation technique, and the chemical stability was analyzed. Meanwhile, the cell biocompatibility and the antibacterial capacities of the coatings against *P. gingivalis* and *S. aureus* were evaluated in vitro.

2. Materials and Methods

2.1. Preparation of Zn-Doped TiO_2 Coating (Zn-MAO)

We gradient polished the pure titanium discs with a diameter of 14 mm (thickness: 1.5 mm) to 1200 mesh. Then, we ultrasonically washed these titanium specimens with acetone and distilled water, and dried at 40 °C. We prepared the Zn-MAO coatings using a DC power supply in constant voltage mode. The MAO electrolyte solution consisted of 20 g/L trisodium phosphate dodecahydrate ($Na_3PO_4 \cdot 12H_2O$), 4 g/L potassium hydroxide (KOH), 10 g/L EDTA disodium, and zinc acetate. We set the concentration of zinc acetate (($CH_3COO)_2Zn$) as 0 g/L, 0.05 g/L, 0.1 g/L, and 0.25 g/L, and recorded them as 0Zn-MAO, 0.05Zn-MAO, 0.1Zn-MAO, and 0.25Zn-MAO, respectively, according to Table 1. During MAO process, we used the stainless-steel plate as the cathode plate and the titanium sample as the anode. We maintained the temperature of electrolyte at 15 °C via circulating water treatment system. We conducted the fabrication under a constant voltage of 400 V for 4 min. After MAO, we washed the specimens with acetone and alcohol, then dried at room temperature.

Table 1. Scheme for preparation coatings.

Name	Electrolyte				Treatment Time (min)	Applied Voltage (V)
	$Na_3PO_4 \cdot 12H_2O$ (g/L)	KOH (g/L)	EDTA (g/L)	$(CH_3COO)_2Zn$ (g/L)		
0Zn-MAO	20	4	10	0	4	400
0.05Zn-MAO	20	4	10	0.05	4	400
0.1Zn-MAO	20	4	10	0.1	4	400
0.25Zn-MAO	20	4	10	0.25	4	400

2.2. Surface Characterization

We observed the surface morphology of the coatings by scanning electron microscope (SEM, Quanta FEG 450, Hillsboro, OR, USA). We analyzed the surface and cross-sectional elemental compositions of the MAO coatings by energy-dispersive X-ray spectroscopy (EDS, Octane SDD, EDAX, Los Angeles, CA, USA). We performed the phase composition of all coatings by X-ray diffraction (XRD, D8 ADVANCE, Bruker, Munich, Germany). We subjected the coatings to X-ray microanalysis system (XPS, ESCALAB 250 Xi, Thermo Scientific, Cambridge, UK) to evaluate the changes in the chemical state of Zinc on the surface of Zn-doped coatings. We analyzed the hydrophilicity of the coatings ($n = 4$) by a contact angle meter (Dataphysics, OCA20, Stuttgart, Germany). We carried out the Zn^{2+} release experiments in saline at 36.5 °C for 0–4 weeks; then, we measured via inductively coupled plasma-optical emission spectrometry (ICP-OES, Optima 5300 DV, Perkin Elmer, Waltham, MA, USA). We measured three samples in each group.

2.3. Cytocompatibility for Zn-Doped Coating (Zn-MAO)

2.3.1. Preparation of Cell

In this study, we used four-week-old Sprague–Dawley (SD) rats to isolate and culture BMSCs. We isolated bone marrow from mice's tibias and suspended it in 10% fetal bovine serum (FBS, Gibco, Carlsbad, CA, USA) and 1% penicillin–streptomycin–amino acids (PS, Gibco). We used an atmosphere of 5% CO_2 and 37 °C to culture the primary cells for 48 h. Following that, we collected BMSCs from the bottom of the dishes. Every three days, we replaced the medium. In the following experiments, we used cells between passage 3 and 6.

2.3.2. Cell Viability Assays

We used a CCK-8 kit to detect the proliferation of BMSCs cultured on the surface of Zn-doped coatings. The seeding density was 7×10^4 cells/mL in 24-well plates. After 1, 3, and 5 days of culture, we measured cytotoxicity. Proliferation trials involved changing the medium every other day. After the prescribed incubation time, we added CCK-8 dye to each well; then, we cultured the plates for another 2 h at 37 °C. At last, we measured the optical density (OD, $n = 5$) at 450 nm by a plate reader. We employed five samples for each coating in the test.

After incubating the cells for 3 days, we washed with PBS, fixed with 4% paraformaldehyde for 10 min at room temperature, and then dehydrated in ethanol for 10 min per gradient, followed by vacuum drying. After gold sputtering, we observed the samples via SEM (Quanta FEG 450) for cell growth morphologies.

2.4. Antibacterial Properties of Zn-Doped Coating (Zn-MAO)

2.4.1. Preparation of Bacteria

We selected *S. aureus* (ATCC25923), the representative species of gram-positive bacteria, as the bacteria for the antibacterial experiment; furthermore, we selected *P. gingivalis* (ATCC 33277) as the representative species of gram-negative bacteria. We cultivated all species with brain heart infusion (BHI). We cultured *P. gingivalis* anaerobically with 80% N_2, 10% H_2, and 10% CO_2, and cultured *S. aureus* aerobically at 37 °C. For each bacterium, we adjusted

the concentration of inoculation to 10^6 colony-forming units and counted CFU/mL for antimicrobial assays.

2.4.2. Plate-Counting Method

We evaluated the antibacterial effects of Zn-doped coatings by the plate-counting method. We inoculated bacteria suspension (200 µL) on the surface of the Zn-MAO coating. We tightly covered the surface of the sample with a sterilized cover-slip to ensure adequate contact between bacteria and samples, and incubated at 37 °C and 5% CO_2 for 24 h. We washed specimens with 1 mL of PBS to remove the bacteria in the cell culture dish.

We evenly spread 50 µL of the remaining bacterial suspension on Columbia AGAR plates and further incubated for 24 h. After that, we counted each group's colony-forming units (CFU). We carried out the experiments three times, and CFU was the average of three results.

We observed the bacterial growth morphology on Zn-MAO by SEM. We washed the bacterial cells with PBS after incubating on the surface for 24 h, fixed with 4% paraformaldehyde for 10 min at room temperature, and then dehydrated in ethanol for 10 min per gradient, followed by vacuum drying. After gold sputtering, we observed the samples via SEM (Quanta FEG 450) for bacterial growth morphologies.

2.5. Statistics

We repeated all assays at least three times. We collected and expressed data as the mean ± standard deviation. We considered statistical significance difference at * $p < 0.05$ and ** $p < 0.01$.

3. Results

3.1. Surface Characterization

Figure 1A shows the surface topography of the coatings deposited in different electrolytes. After the MAO process, volcano-shaped microporous TiO_2 coatings were prepared on the surface of pure titanium. There was no obvious difference in the porous microstructure after the incorporation of Zn. The XRD spectra of Zn-doped coatings are presented in Figure 1B. They revealed the presence of only anatase and rutile phases in Zn-doped coatings without any Zn-related phase. Therefore, the Zn-existing states in Zn-doped coatings should be further analyzed using a high-resolution XPS spectrum.
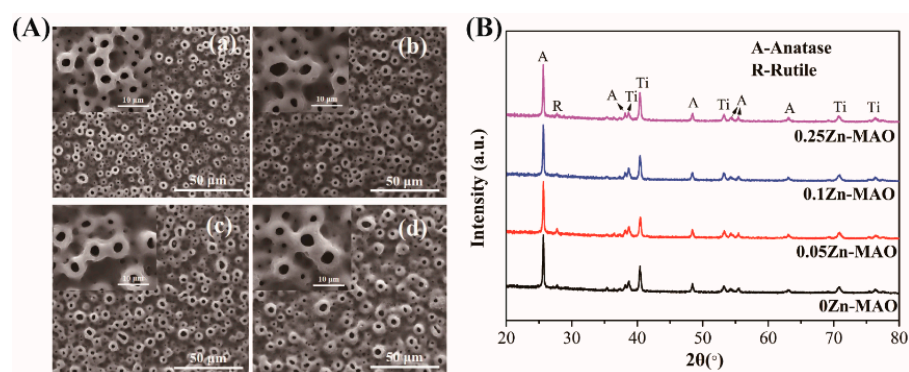
Figure 1. Surface morphologies of different coatings (**A**): (**a**) 0Zn-MAO, (**b**) 0.05Zn-MAO, (**c**) 0.1Zn-MAO, (**d**) 0.25Zn-MAO. XRD patterns of different coatings (**B**).

The chemical compositions of the coatings were clearly revealed from the XPS full spectrum (Figure 2a). The Ti, O, and P were detected on all the surfaces. The high-resolution XPS spectra of Zn obtained from 0.05Zn-MAO, 0.1Zn-MAO, and 0.25Zn-MAO are shown in Figure 2b. Two peaks centered at 1044.4 and 1021.5 eV emerged in the high-resolution spectra for Zn2p, which revealed the presence of Zn^{2+} in the Zn-doped coating.
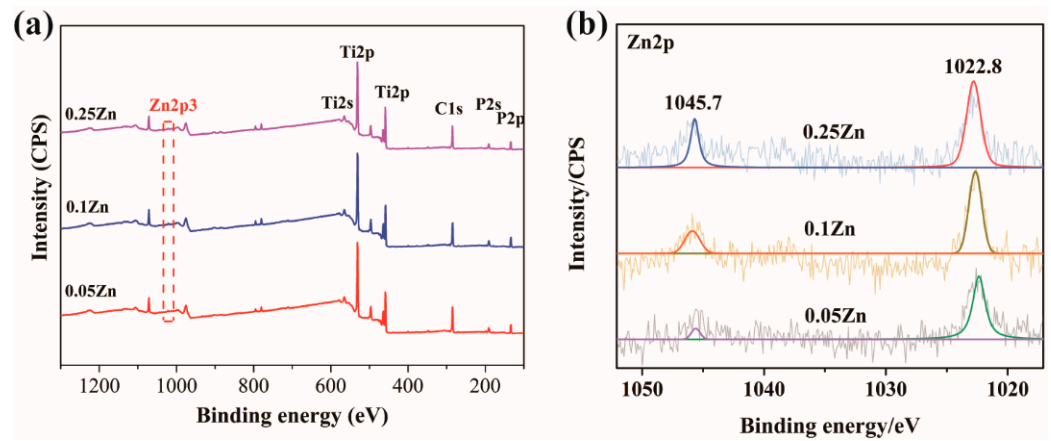
Figure 2. XPS survey spectrum (**a**) and Zn2p high-resolution spectra of the 0.05Zn-MAO, 0.1Zn-MAO and 0.25Zn-MAO coatings (**b**).

Table 2 presents the concentration estimated by EDS. As concentrations of Zinc acetate added in the electrolyte increased, the amount of Zn increased from 0.45 wt.% (0.05Zn-MAO) to 3.45 wt.% (0.25Zn-MAO). This indicated that the Zn content in the coating can be adjusted by adjusting the concentration of the Zinc acetate in the electrolyte. Figure 3a–d show the cross-sectional SEM morphologies of the Zn-doped coatings. It can be seen that all the coatings have a cross-sectional thickness of 4–7 µm. The chemical composition of the 0.25Zn-MAO coating was examined by EDS. Figure 3e is the line-scan analysis along the yellow arrow in Figure 3d. This indicated that the Zn element is distributed throughout the thickness of the coating.

Table 2. Element component (wt.%) on the surface of different coatings.

Sample	Element Component (wt.%)			
	Ti	Zn	O	P
0Zn	73.08	-	16.06	34.85
0.05Zn	73.34	0.45	17.49	8.72
0.1Zn	74.27	1.26	14.67	9.8
0.25Zn	70.52	3.45	16.62	9.41
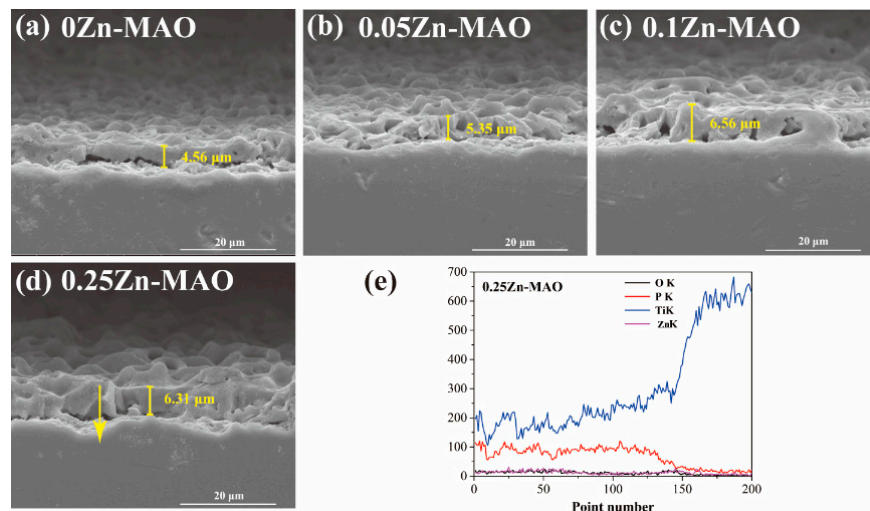
Figure 3. Cross-sectional SEM morphologies of 0Zn-MAO (**a**), 0.05Zn -MAO (**b**), 0.1Zn-MAO (**c**), and 0.25ZN-MAO (**d**) coatings, and EDS line-scan analysis crossing the yellow arrow marked in Zn-doped coatings in (**e**).

As shown in Figure 4a, the contact angle of 0Zn-MAO was 43°. With the increase of Zinc acetate in the electrolyte, the contact angle of the coating also increased linearly. However, the contact angles of the Zn-doped coatings were in the range of 43–49°, which indicated that adding Zn did not obviously alter their hydrophilicity. ICP-OES detected the release of Zn^{2+} at different time points. The amount of Zn released from the Zn-MAO coating as a function of immersion time in 0.9 wt.% NaCl solution at 36.5 °C was measured, and the result was shown in Figure 4b. The release curve shows that the release of Zn is slow and continuous in the prolonged immersion process.
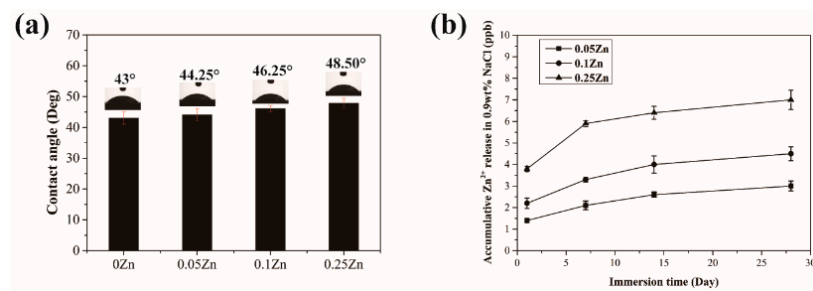
Figure 4. Contact angles of Zn-MAO coatings (**a**). The release of Zn^{2+} from 0.05Zn-MAO, 0.1Zn, and 0.25Zn groups on 1, 7, 14, and 28 days (**b**).

### 3.2. The Cell Biocompatibility of Zn-MAO Coating

The cell viability was tested by CCK-8, the result of which showed the OD value was increased significantly in the 0Zn-MAO, 0.05Zn-MAO, 0.1Zn-MAO, and 0.25Zn-MAO groups at 5 days ($p < 0.05$) (Figure 5a). Compared with the Ti group, the Zn-doped groups showed much higher viability at 3 and 5 days. As shown in Figure 5b, the cell morphologies on different coatings after incubation for 3 days were observed by SEM. Compared with Ti, the cells attach and spread better on the surface of 0Zn-MAO and 0.25Zn-MAO. On Ti, the cells are spherical and spread less, whereas on 0Zn-MAO and 0.25Zn-MAO, the cells are polygonal and covered the pores. All the results present the good cell biocompatibility of Zn-MAO coatings in our study.
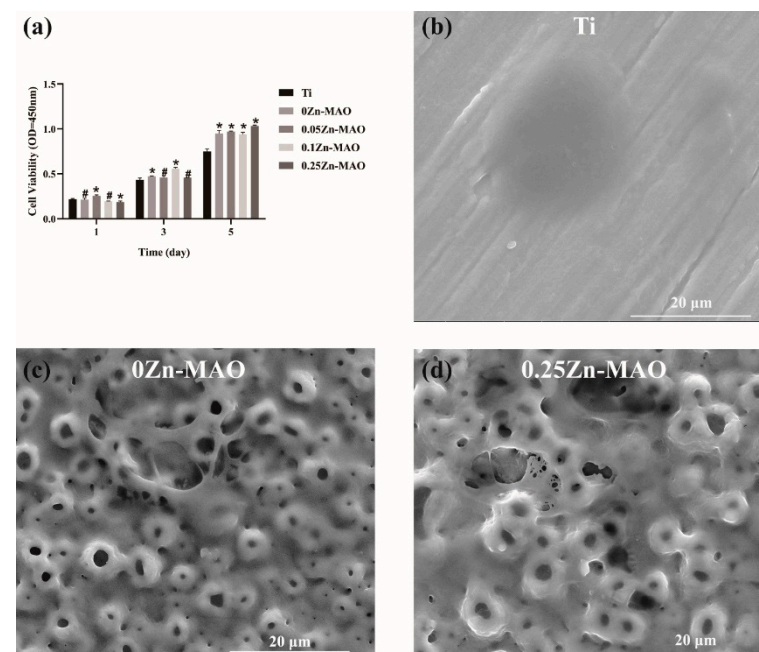
Figure 5. The cell biocompatibility of Zn-MAO (**a**). Cytotoxicity was measured after 1, 3, and 5 days of culture. The BMSCs morphologies on Ti (**b**), 0Zn (**c**), and 0.25Zn (**d**) groups surface for 3 days under SEM. Data are presented as mean ± SD; (* $p < 0.05$, # $p > 0.05$, vs. Ti group).

3.3. Antibacterial Properties of Zn-MAO Coating

Figure 6a,b show images of *S. aureus* and *P. gingivalis* colonies cultured on the Zn-MAO coatings for 24 h. We found that the plates corresponding to the 0.25Zn coating had the lowest bacteria colony numbers compared to the other coatings. It revealed that the 0.25Zn-MAO coating exhibits powerful antibacterial activities. As showed in Figure 6c, the effects of those Zn-MAO coatings on bacterial morphology and cell-wall integrity were observed via SEM. The *P. gingivalis* and *S. aureus* grown on the surface of 0Zn-MAO coating are rounded with integrated membranes, while there were some bacteria collapsed, corrugated, and fractured on the surface of Zn-MAO coatings (marked with arrows in Figure 6c).
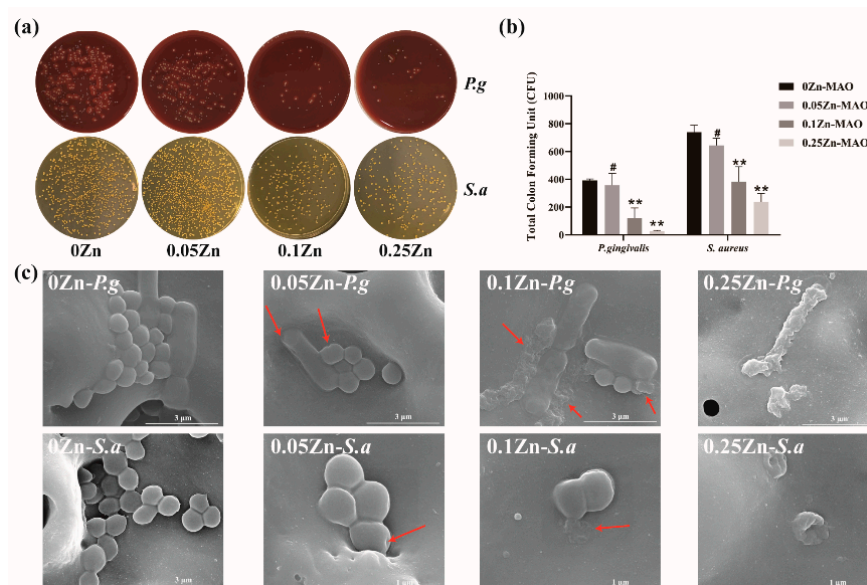

Figure 6. Antibacterial activities of Zn-doped coatings against *S. aureus* and *P. gingivalis* (**a**); CFU results after *S. aureus* and *P. gingivalis* were cocultured with the Zn-MAO coating for 24 h (**b**). The SEM images (**c**) of *S. aureus* and *P. gingivalis* cultured on different surface after 24 h of incubation. Data are presented as mean $\pm$ SD; (** $p < 0.01$, # $p > 0.05$, vs. 0Zn-MAO group).

4. Discussion

After an implant is implanted in the body, the surface of the materials undergo a series of biochemical reactions, and the structure of the material surface plays a crucial role in the implant's response to the internal environment. The microstructure and chemical composition of the implant surface can modify the adsorption of proteins that regulate cell adhesion and ultimately determine its function [27].

In our study, MAO coatings were prepared on pure titanium, and pores of a microscale size were distributed, as shown in Figure 1A. The microscale pores can significantly promote cell adhesion and osteogenic differentiation [28]. In addition, the volcano-shaped microporous surface can provide the required spatial environment for the growth of different cells, thus promoting the proliferation and adhesion of most osteoblasts on the surface of the material [29,30]. During the MAO process, a large number of micro-arcs struck over the anode surface, and the microscale pores are believed to be the discharge channels of these arcs [31]. It can be seen from the XRD results (Figure 1B) that the Zn-doped coatings comprised mainly anatase. Some anatase converted to rutile due to the high temperatures accompanying grain growth [32]. Many studies reported that anatase has unique features and advantages in medical applications. It also can absorb more OH^- and PO_4^{3-}, which is favorable for the deposition of bone-like apatite in body fluids [10,33,34]. MAO treatment can only incorporate this element into the resulting oxide coating when the element is dissolved in the electrolyte [35,36]. In addition, phosphorus (P) is the bio-functional ion, while Zn is the essential trace element for human beings. Bacteria can be inhibited from adhering and reproducing [37]. The data via EDS analysis demonstrated that O, P, and

Zn in the electrolyte are ultimately deposited throughout the MAO coatings (Table 1 and Figure 2). During the MAO process, the oxygen from the electrolyte was transported to the titanium substrate through the discharge channel to form TiO_2 [38]. At the same time, the Zn^{2+} from the zinc acetate combined with the EDTA to form negatively charged complexes. These zinc-containing complexes then moved toward the anode, mainly by electromigration. The Zn^{2+} binding with PO_4^{3-} from trisodium phosphate dodecahydrate formed $Zn_3(PO_4)_2$ in the end [39]. The main reactions of Zn^{2+} deposition may be described as follows:

$$Zn^{2+} + EDTA^{4-} = ZnEDTA^{2-} \tag{1}$$

$$Na_3PO_4 = 3Na^+ + PO_4^{3-} \tag{2}$$

$$Na_3PO_4 = 3Na^+ + PO_4^{3-} \tag{3}$$
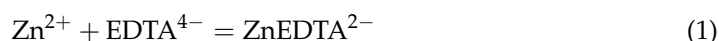
The contact angles of the Zn-doped MAO coatings were from 43° to 48.5° (data in brief, Figure 4a), which shows hydrophilicity. Hydrophilic surfaces are beneficial in the early phases of osseointegration [40], which will be suitable for cell adhesion on the implant surface. The cell viability of BMSCs on Zn-MAO coatings was much higher than in the Ti group (Figure 5a), which proved that Zn-MAO coatings were more appropriate and suitable for BMSCs proliferation. In conclusion, the Zn-MAO coating possesses good cell biocompatibility in our study.

The antimicrobial coating on the surface of the implant is a method for preventing peri-implantitis. Antibacterial elements, such as Ag, Cu, and Zn, are easily used to incorporate onto the Ti surface to generate an antibacterial surface by MAO. The verifications have illustrated that the incorporation of Zn possesses certain antibacterial capabilities, and has been extensively used to improve the antibacterial abilities of implants [41,42]. In our study, Zn was chosen to incorporate into the TiO_2 layer by the application of different concentrations of zinc acetate via the MAO electrolyte.

S. aureus is a frequent commensal of the nares and skin and is considered a transient oral resident, which is found identified at higher numbers in biofilm obtained from implants with peri-implantitis than peri-implant health [23]. *P. gingivalis* is recognized as most closely related to the development of peri-implantitis and even the ultimate loss of implants [22]. Therefore, *S. sanguinis* and *P. gingivalis* were selected as representative strains for peri-implantitis-associated biofilm experiments in vitro. Figure 6a shows the 0.25Zn-MAO coating achieved greater inhibition against two types of single-species biofilms by the CFU. The antibacterial rates of 0.25Zn-MAO coating against *S.aureus* and *P. gingivalis* bacterial were 68% and 93.4%, respectively. It indicated that the 0.25Zn-MAO coating possessed a strong bactericidal effect on *P. gingivalis*. SEM results visualized the collapse of *S.aureus* and *P. gingivalis* bacterial structures and the death of bacteria on Zn-MAO coatings. All of these suggest that the 0.25Zn-MAO coatings showed an excellent antibacterial effect on the peri-implant inflammatory pathogens. The antibacterial mechanism for Zn-MAO coating could be explained as through a mechanism of damaging bacterial cell membranes by the generation of reactive oxygen species [43,44]. It can not only penetrate the membrane of bacteria and interact with proteins but also damage the DNA of bacteria and prevent the proliferation of bacteria [45].

5. Conclusions

In this study, Zn-doped porous TiO_2 coatings were prepared on the surface of titanium by MAO. The structures of Zn-doped coatings were systematically investigated. To evaluate the antibacterial effect of Zn-doped coatings, we cultured the gram-negative (*P. gingivalis*) and gram-positive bacteria (*S. aureus*) on the surface of Zn-doped coatings. The results showed that 0.25Zn-MAO coatings had the best antibacterial effect. Meanwhile, we found that 0.25Zn-MAO coatings had the best bioactivity, cell proliferation promotion, and adhesion effects relative to Ti and 0Zn-MAO through in vitro study. In conclusion, the Zn-doped TiO_2 coatings had good biocompatibility and antimicrobial properties, which may be helpful in eradicating biomaterial-associated infections.

References

1. Hanawa, T. Titanium-Tissue Interface Reaction and Its Control with Surface Treatment. *Front. Bioeng. Biotechnol.* **2019**, *7*, 170. [CrossRef] [PubMed]
2. Shimabukuro, M. Antibacterial Property and Biocompatibility of Silver, Copper, and Zinc in Titanium Dioxide Layers Incorporated by One-Step Micro-Arc Oxidation: A Review. *Antibiotics* **2020**, *9*, 716. [CrossRef] [PubMed]
3. Paquette, D.W.; Brodala, N.; Williams, R.C. Risk factors for endosseous dental implant failure. *Dent. Clin. N. Am.* **2006**, *50*, 361–374. [CrossRef] [PubMed]
4. Smeets, R.; Henningsen, A.; Jung, O.; Heiland, M.; Hammacher, C.; Stein, J.M. Definition, etiology, prevention and treatment of peri-implantitis—A review. *Head Face Med.* **2014**, *10*, 34. [CrossRef]
5. Durdu, S.J.C. Characterization, Bioactivity and Antibacterial Properties of Copper-Based TiO_2 Bioceramic Coatings Fabricated on Titanium. *Coatings* **2018**, *9*, 1. [CrossRef]
6. Khanna, R.; Kokubo, T.; Matsushita, T.; Nomura, Y.; Nose, N.; Oomori, Y.; Yoshida, T.; Wakita, K.; Takadama, H. Novel artificial hip joint: A layer of alumina on Ti-6Al-4V alloy formed by micro-arc oxidation. *Mater. Sci. Eng. C Mater. Biol. Appl.* **2015**, *55*, 393–400. [CrossRef]
7. Li, L.H.; Kong, Y.M.; Kim, H.W.; Kim, Y.W.; Kim, H.E.; Heo, S.J.; Koak, J.Y. Improved biological performance of Ti implants due to surface modification by micro-arc oxidation. *Biomaterials* **2004**, *25*, 2867–2875. [CrossRef]
8. Han, Y.; Chen, D.; Sun, J.; Zhang, Y.; Xu, K. UV-enhanced bioactivity and cell response of micro-arc oxidized titania coatings. *Acta Biomater.* **2008**, *4*, 1518–1529. [CrossRef]
9. Xiu, P.; Jia, Z.; Lv, J.; Yin, C.; Cheng, Y.; Zhang, K.; Song, C.; Leng, H.; Zheng, Y.; Cai, H.; et al. Tailored Surface Treatment of 3D Printed Porous Ti6Al4V by Microarc Oxidation for Enhanced Osseointegration via Optimized Bone In-Growth Patterns and Interlocked Bone/Implant Interface. *ACS Appl. Mater. Interfaces.* **2016**, *8*, 17964–17975. [CrossRef]
10. Akin, F.A.; Zreiqat, H.; Jordan, S.; Wijesundara, M.B.; Hanley, L. Preparation and analysis of macroporous TiO_2 films on Ti surfaces for bone-tissue implants. *J. Biomed. Mater. Res.* **2001**, *57*, 588–596. [CrossRef]
11. Webster, T.J.; Ergun, C.; Doremus, R.H.; Siegel, R.W.; Bizios, R. Enhanced functions of osteoblasts on nanophase ceramics. *Biomaterials* **2000**, *21*, 1803–1810. [CrossRef]
12. Hu, H.; Liu, X.; Ding, C. Preparation and in vitro evaluation of nanostructured TiO_2/TCP composite coating by plasma electrolytic oxidation. *J. Alloy. Compd.* **2010**, *498*, 172–178. [CrossRef]
13. Zhang, B.; Li, B.; Gao, S.; Li, Y.; Cao, R.; Cheng, J.; Li, R.; Wang, E.; Guo, Y.; Zhang, K.J.M. Y-doped TiO_2 coating with superior bioactivity and antibacterial property prepared via plasma electrolytic oxidation. *Mater. Des.* **2020**, *192*, 108758. [CrossRef]
14. Yamamura, K.; Iwata, H.; Yotsuyanagi, T. Synthesis of antibiotic-loaded hydroxyapatite beads and in vitro drug release testing. *J. Biomed. Mater. Res.* **1992**, *26*, 1053–1064. [CrossRef]
15. Shirai, T.; Shimizu, T.; Ohtani, K.; Zen, Y.; Takaya, M.; Tsuchiya, H. Antibacterial iodine-supported titanium implants. *Acta Biomater.* **2011**, *7*, 1928–1933. [CrossRef]
16. Lishchynskyi, O.; Shymborska, Y.; Stetsyshyn, Y. Passive antifouling and active self-disinfecting antiviral surfaces. *Chem. Eng. J.* **2022**, *446*, 137048. [CrossRef]
17. Zhang, L.; Guo, J.; Yan, T.; Han, Y.J.A.S.S. Fibroblast responses and antibacterial activity of Cu and Zn co-doped TiO_2 for percutaneous implants. *Appl. Surf. Sci.* **2018**, *434*, 633–642. [CrossRef]
18. Zhu, H.; Jin, G.; Cao, H.; Qiao, Y.; Liu, X. Influence of implantation voltage on the biological properties of zinc-implanted titanium. *Surf. Coat. Technol.* **2017**, *312*, 75–80. [CrossRef]
19. Hu, H.; Zhang, W.; Qiao, Y.; Jiang, X.; Liu, X.; Ding, C. Antibacterial activity and increased bone marrow stem cell functions of Zn-incorporated TiO_2 coatings on titanium. *Acta Biomater.* **2012**, *8*, 904–915. [CrossRef]

20. Ye, J.; Li, B.; Li, M.; Zheng, Y.; Wu, S.; Han, Y. ROS induced bactericidal activity of amorphous Zn-doped titanium oxide coatings and enhanced osseointegration in bacteria-infected rat tibias. *Acta Biomater.* **2020**, *107*, 313–324. [CrossRef]

21. Zhao, B.H.; Zhang, W.; Wang, D.N.; Feng, W.; Liu, Y.; Lin, Z.; Du, K.Q.; Deng, C.F. Effect of Zn content on cytoactivity and bacteriostasis of micro-arc oxidation coatings on pure titanium. *Surf. Coat. Technol.* **2013**, *228*, S428–S432. [CrossRef]

22. Qi, H.; Li, B.; Wang, H.; Cai, Q.; Quan, X.; Cui, Y.; Meng, W. Effects of d-valine on periodontal or peri-implant pathogens: *Porphyromonas gingivalis* biofilm. *J. Periodontol.* **2018**, *89*, 303–314. [CrossRef]

23. Zhuang, L.F.; Watt, R.M.; Mattheos, N.; Si, M.S.; Lai, H.C.; Lang, N.P. Periodontal and peri-implant microbiota in patients with healthy and inflamed periodontal and peri-implant tissues. *Clin. Oral. Implant. Res.* **2016**, *27*, 13–21. [CrossRef]

24. Renvert, S.; Aghazadeh, A.; Hallström, H.; Persson, G. Factors related to peri-implantitis–a retrospective study. *Clin. Oral. Implant. Res.* **2014**, *25*, 522–529. [CrossRef]

25. Harris, L.; Richards, R. Staphylococcus aureus adhesion to different treated titanium surfaces. *J. Mater. Sci. Mater. Med.* **2004**, *15*, 311–314. [CrossRef]

26. Costerton, J.W.; Montanaro, L.; Arciola, C.R. Biofilm in implant infections: Its production and regulation. *Int. J. Artif. Organs.* **2005**, *28*, 1062–1068. [CrossRef]

27. Wang, L.J.; Ni, X.H.; Zhang, F.; Peng, Z.; Yu, F.X.; Zhang, L.B.; Li, B.; Jiao, Y.; Li, Y.K.; Yang, B. Osteoblast Response to Copper-Doped Microporous Coatings on Titanium for Improved Bone Integration. *Nanoscale Res. Lett.* **2021**, *16*, 146. [CrossRef]

28. Zhou, W.; Huang, O.; Gan, Y.; Li, Q.; Zhou, T.; Xi, W. Effect of titanium implants with coatings of different pore sizes on adhesion and osteogenic differentiation of BMSCs. *Artif. Cells Nanomed. Biotechnol.* **2019**, *47*, 290–299. [CrossRef]

29. Gittens, R.A.; McLachlan, T.; Olivares-Navarrete, R.; Cai, Y.; Berner, S.; Tannenbaum, R.; Schwartz, Z.; Sandhage, K.H.; Boyan, B.D. The effects of combined micron-/submicron-scale surface roughness and nanoscale features on cell proliferation and differentiation. *Biomaterials* **2011**, *32*, 3395–3403. [CrossRef]

30. Li, X.; Wang, M.; Zhang, W.; Bai, Y.; Liu, Y.; Meng, J.; Zhang, L. A Magnesium-Incorporated Nanoporous Titanium Coating for Rapid Osseointegration. *Int. J. Nanomed.* **2020**, *15*, 6593–6603. [CrossRef]

31. Mi, T.; Jiang, B.; Liu, Z.; Fan, L. Plasma formation mechanism of microarc oxidation. *Electrochim. Acta.* **2014**, *123*, 369–377. [CrossRef]

32. Tang, G.-X.; Zhang, R.-J.; Yan, Y.-N.; Zhu, Z.-X. Preparation of porous anatase titania film. *Mater. Lett.* **2004**, *58*, 1857–1860. [CrossRef]

33. Nie, X.; Leyland, A.; Matthews, A.; Jiang, J.C.; Meletis, E.I. Effects of solution pH and electrical parameters on hydroxyapatite coatings deposited by a plasma-assisted electrophoresis technique. *J. Biomed. Mater. Res.* **2001**, *57*, 612–618. [CrossRef]

34. Yerokhin, A.L.; Nie, X.; Leyland, A.; Matthews, A. Characterisation of oxide films produced by plasma electrolytic oxidation of a Ti–6Al–4V alloy. *Surf. Coat. Technol.* **2000**, *130*, 195–206. [CrossRef]

35. Ha, J.Y.; Tsutsumi, Y.; Doi, H.; Nomura, N.; Kim, K.H.; Hanawa, T. Enhancement of calcium phosphate formation on zirconium by micro-arc oxidation and chemical treatments. *Surf. Coat. Technol.* **2011**, *205*, 4948–4955. [CrossRef]

36. Shimabukuro, M.; Tsutsumi, H.; Tsutsumi, Y.; Manaka, T.; Chen, P.; Ashida, M.; Ishikawa, K.; Katayama, H.; Hanawa, T. Enhancement of antibacterial property of titanium by two-step micro arc oxidation treatment. *Dent. Mater. J.* **2021**, *40*, 592–598. [CrossRef]

37. Mirastschijski, U.; Martin, A.; Jorgensen, L.N.; Sampson, B.; Agren, M.S. Zinc, copper, and selenium tissue levels and their relation to subcutaneous abscess, minor surgery, and wound healing in humans. *Biol. Trace. Elem. Res.* **2013**, *153*, 76–83. [CrossRef]

38. Curran, J.A.; Clyne, T.W. Porosity in plasma electrolytic oxide coatings. *Acta Mater.* **2006**, *54*, 1985–1993. [CrossRef]

39. Liu, J.; Zhu, R.; Xu, T.; Xu, Y.; Ge, F.; Xi, Y.; Zhu, J.; He, H. Co-adsorption of phosphate and zinc(II) on the surface of ferrihydrite. *Chemosphere* **2016**, *144*, 1148–1155. [CrossRef]

40. Buser, D.; Broggini, N.; Wieland, M.; Schenk, R.; Denzer, A.; Cochran, D.; Hoffmann, B.; Lussi, A.; Steinemann, S. Enhanced bone apposition to a chemically modified SLA titanium surface. *J. Dent. Res.* **2004**, *83*, 529–533. [CrossRef]

41. Reddy, L.S.; Nisha, M.M.; Joice, M.; Shilpa, P.N. Antimicrobial activity of zinc oxide (ZnO) nanoparticle against *Klebsiella pneumoniae*. *Pharm. Biol.* **2014**, *52*, 1388–1397. [CrossRef]

42. Xie, Y.; He, Y.; Irwin, P.L.; Jin, T.; Shi, X. Antibacterial activity and mechanism of action of zinc oxide nanoparticles against Campylobacter jejuni. *Appl. Environ. Microbiol.* **2011**, *77*, 2325–2331. [CrossRef]

43. San Miguel, S.M.; Opperman, L.A.; Allen, E.P.; Zielinski, J.E.; Svoboda, K.K. Antioxidant combinations protect oral fibroblasts against metal-induced toxicity. *Arch. Oral. Biol.* **2013**, *58*, 299–310. [CrossRef]

44. Gudkov, S.V.; Burmistrov, D.E.; Serov, D.A. A Mini Review of Antibacterial Properties of ZnO Nanoparticles. *Front. Phys.* **2021**, *9*, 641481. [CrossRef]

45. Tsutsumi, H.; Tsutsumi, Y.; Shimabukuro, M. Investigation of the long-term antibacterial properties of titanium by two-step micro-arc oxidation treatment. *Coating* **2021**, *11*, 798. [CrossRef]